Please answer all sections of the document. You are welcome to use figures and tables to complement or enhance the text. For annual reports, please only describe work for the period of performance (July 1, 2014 - June 30, 2015). For final reports, please describe the comprehensive effort.

Grant/Award #: IACRO 13-5897I (previous id's: 12-2026I, 11-4471I, 10-4257I)
PI Name: David P. Adams
Organization/Institution: Sandia National Laboratories
Project Title: Basic Research of Intrinsic, Tamper Indication Markings and Patterns Defined by Pulsed Laser Irradiation

What are the major goals of the project?
List the major goals of the project as stated in the approved application or as approved by the agency. If the application lists milestones/target dates for important activities or phases of the project, identify these dates and show actual completion dates or the percentage of completion. Generally, the goals will not change from one reporting period to the next. However, if the awarding agency approved changes to the goals during the reporting period, list the revised goals and objectives. Also explain any significant changes in approach or methods from the agency-approved application or plan.

The goals of the current year are as follows:

Task 7: Research of microspectrophotometry for inspection and validation of laser color markings

Task 8: Investigate new laser fabrication techniques that produce color markings with improved corrosion resistance

Task 9: Research new methods for laser marking curved surfaces (and large areas)

Task 10: Complete model simulations of laser-induced ripple formation – involves an ElectroMagnetic field solver

Sandia National Laboratories

Sandia National Laboratories is a multimission laboratory managed and operated by National Technology & Engineering Solutions of Sandia, LLC, a wholly owned subsidiary of Honeywell International Inc., for the U.S. Department of Energy's National Nuclear Security Administration under contract DE-NA0003525.

Sandia National Laboratories is a multi-program laboratory managed and operated by Sandia Corporation, a wholly owned subsidiary of Lockheed Martin Company, for the United States Department of Energy's National Nuclear Security Administration under Contract DE-AC04-94AL85000.

What was accomplished under these goals?
For this reporting period describe: 1) major activities; 2) specific objectives; 3) significant results, including major findings, developments, or conclusions (both positive and negative); and 4) key outcomes or other achievements. Include a discussion of stated goals not met. As the project progresses, the emphasis in reporting in this section should shift from reporting activities to reporting accomplishments.

Task 7: Research of microspectrophotometry for inspection and validation of laser color markings

Background:

In a previous year of this DTRA-funded research, our team showed that laser-colored areas exhibit an average color set by the accumulated fluence used in the experiment; however, many marked areas also contained embedded, color islands. Islands exhibit a different color compared with neighboring areas, at least when observed in an optical microscope. Therefore, they are another form of intrinsic marking that could be cataloged for asset identification and protection. Detailed analysis showed that micro-scale islands form at randomly placed sites (within a uniformly-irradiated area) and likely originate at exposed precipitates, certain grain boundaries or other surface features. An optical image of islands is included in Figure 1.

Although optical microscopy shows qualitative color differences amongst islands and surrounding material, optical microscopy does not quantify spectral variations. Certainly, optical microscopy is useful pinpointing the locations and relative spacing and sizes of color islands; this can be referenced to a fiducial or coordinate system for cataloging. Nevertheless, our team desired to investigate ways in which the spectral reflectance of microscopic, color islands could be evaluated for the purpose of cataloging (akin to a fingerprint pattern). It is thought that a map of the random island locations and their individual spectral characteristics are virtually impossible to reproduce even when using an identical laser process applied to a surface of identical starting surface roughness.

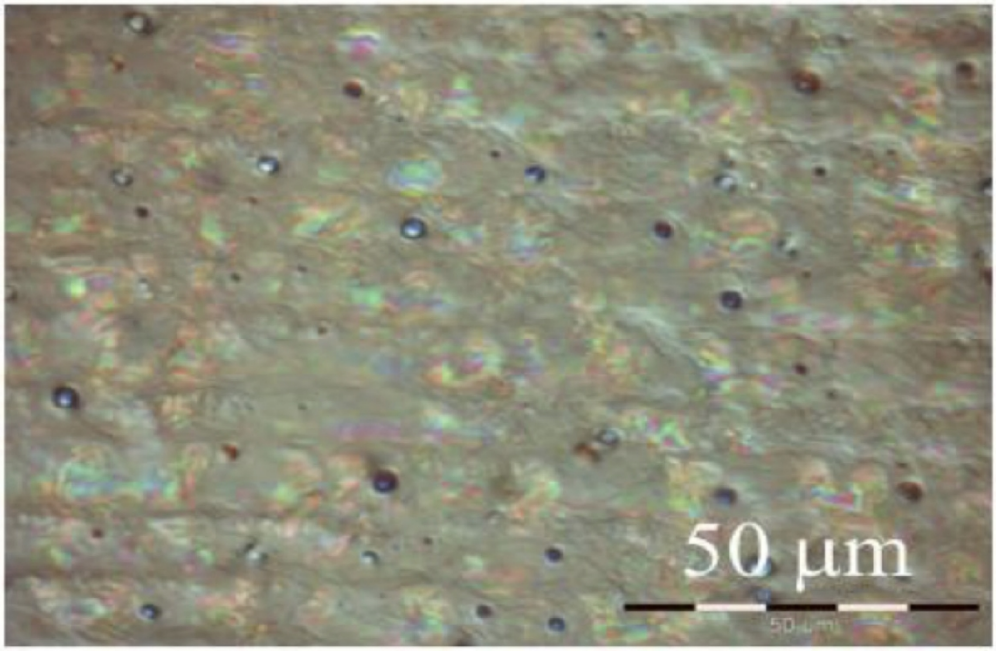

Figure 1. Optical micrographs (included in previous year-end report) showing isolated color features (islands) within area uniformly treated by laser irradiation in air. The islands are shown to exhibit different colors.

Major activities:

In the past year we have investigated a new, non-contact, light-based method (UV-Vis-IR microspectrophotometry) for rapid interrogation of color island spectral signature. The instrument selected for investigation is a commercially available microspectrometer from CRAIC, Inc. A picture of this benchtop instrument is included in Figure 2. It is designed to determine the spectral reflectance of microscopic planar areas. In our study, we evaluate whether it is capable of differentiating the spectral response of micro-color islands versus the average patterned area. By spectral reflectance, we specifically mean the reflectance over a range of different wavelengths. A 20X objective is used for both identifying regions of interest and for evaluating spectral response of individual microscopic areas within the field of view. The OEM claims that the instrument is calibrated using filters that were traceable to Standard Reference Materials from NIST.

A major activity of this study included determining the spectral response of colored islands and determining whether these are different than surrounding laser treated areas as suggested using the optical microscope. A range of wavelengths from 200 to 1500 nm is available for study. The spectral resolution of this instrument is quoted at better than 1 nm. Color islands are generally small, ~ 10 microns in diameter, as shown in Figure 1. Therefore, another important aspect of study was to determine if the

small features could be evaluated. Laser color markings produced on stainless steel were chosen for study involving the microspectro-photometer. Samples were made using two different accumulated laser fluences (200 and 1000 J/cm^2). Areas patterned by the laser were each 4 x 4 mm.

Another activity supported under this task is the detailed study of the optical constants (n and k) of produced oxide lasers. This basic research was conducted to better understand the mechanisms underlying color formation in laser treated samples. In the past ten months, studies of optical constants have involved microbeam, spectroscopic ellipsometry (instrument is shown in Figure 3 below). Samples investigated in the past few months include oxides produced on Cr, V and Ti metal films. All metal films were initially deposited by sputter methods. Afterwards, the laser was scanned over the films in air to produce oxide capping layers of different thickness and color. In all cases, laser color marked films remained well adhered to underlying substrates. Results derived from ellipsometry were correlated with microstructure, composition and morphology revealed by electron microscopy and Auger electron spectroscopy to arrive at explanations for colored appearance.

Figure 2. Benchtop microspectrophotometer (CRAIC) used for the evaluation of color islands on laser marked, bulk stainless steel 304L samples. Image from CRAIC website.

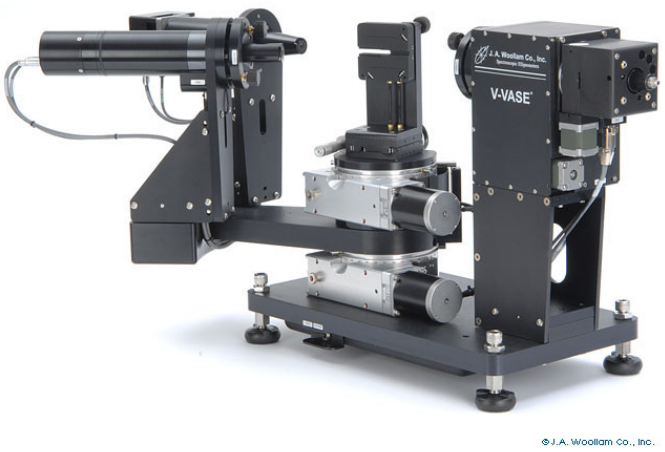

Figure 3. Benchtop, variable angle, spectroscopic ellipsometer (Woollam, Inc.) used in this study of optical constants for laser color marked samples. Image from Woollam website.

Specific Objective(s):

The specific objective for the previous year was the following:

- Research of microspectrophotometry for inspection / validation of laser color markings (Task 7)

Significant Results and Findings:

Laser-color markings produced on stainless steel (bulk) samples were evaluated by UV-Vis-IR microspectrophotometry. First, samples produced with no color islands (such as that shown in Figure 4 made using a fluence of 200 J/cm^2) was scanned to determine spectral reflectance point-by-point. Areas such as the 10 x 10 micron area highlighted with a red-outlined box in this figure were evaluated over a range of wavelengths from 400 to 700 nm. This particular box spans across two laser lines. The left-to-right oriented lines in Figure 4 are artifacts of the scanned beam that was moved across to defined a color feature in this area.

As demonstrated with a few representative scans in Figure 5, this method proved useful for determining the minor color variations across this particular planar surface. The particular wavelength listed to the right of the color map was that used to determine the reflectance variations across the area of interest specific to that incident waveform. Sample acquisition time was rapid with 10 x 10 micron areas requiring seconds.

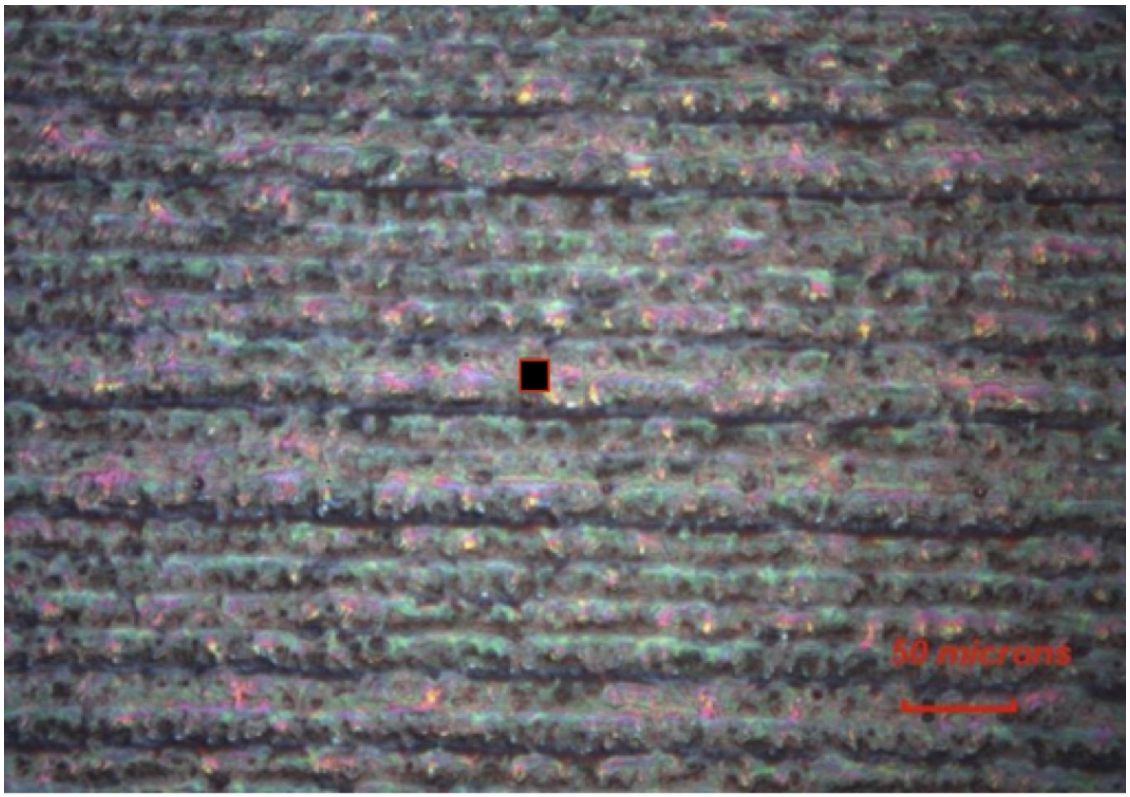

Figure 4. Optical image of a laser colored area that has not formed colored islands. This entire area was sampled using the UV-Vis-IR microspectrophotometer. The microscopic area shown with a red outlined box was sampled to produce the spatially-resolved reflectance/color maps included below.

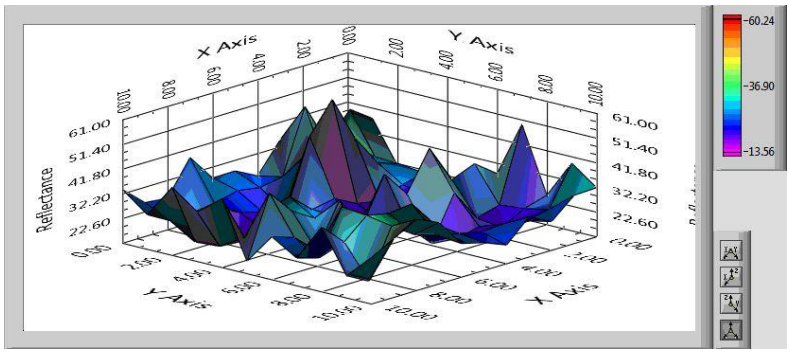

λ = 700 nm

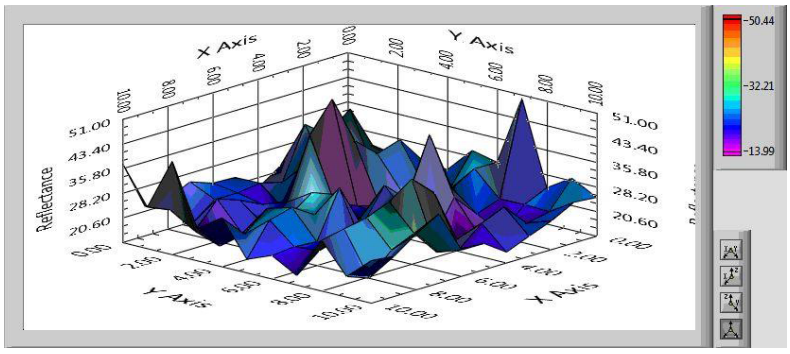

λ = 650 nm

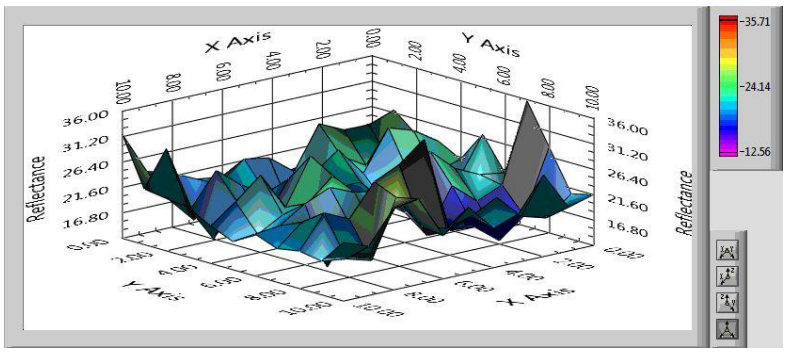

λ = 600 nm

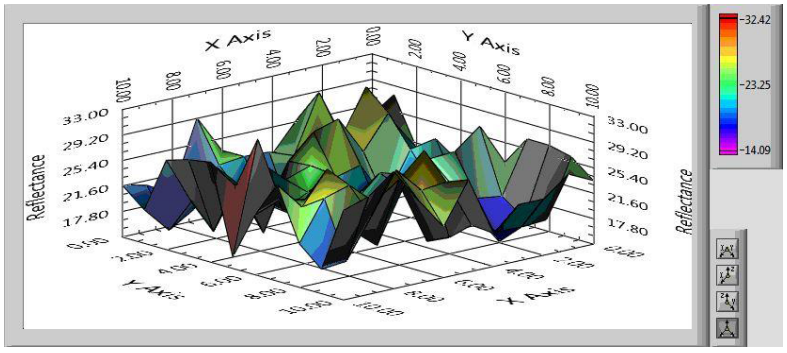

λ = 550 nm

Figure 5. Spatially resolved color/reflectance maps of a laser-treated stainless steel sample. Little variation is found across the 10 x 10 micron area. No color islands were present on this sample's surface.

Additional, laser-color marked stainless steel samples comprised of microscale color islands were also evaluated using the same method in order to determine if islands could be identified and, if so, whether they exhibit unique spectral reflectance. The image in Figure 6 shows an area treated with a single, uniform laser fluence. The microscopic area highlighted with a red-outlined box was selected for demonstration. Within the upper right corner of this microscopic sampling area, a color island is included for comparison. This is shown in more with a high magnification view in the bottom image of Figure 6.

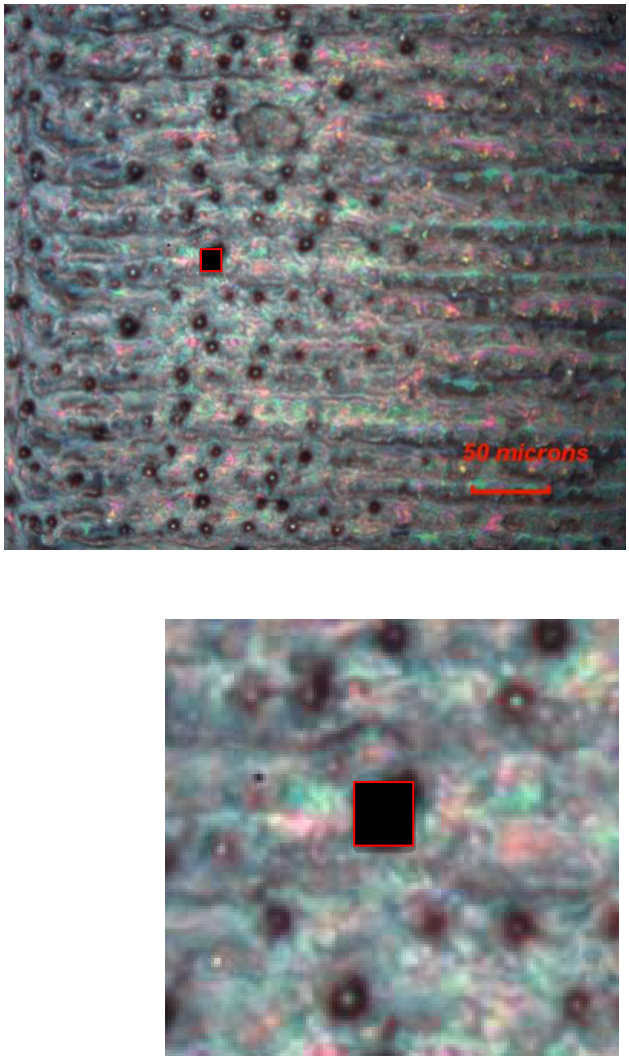

Figure 6. Optical images of a laser colored area having embedded, color islands of dimension 5-10 microns on average. The highlighted area was sampled using the UV-Vis-IR microspectrophotometer to produce the spatially-resolved reflectance maps included in Figure 7. Note, this area partially includes a color island.

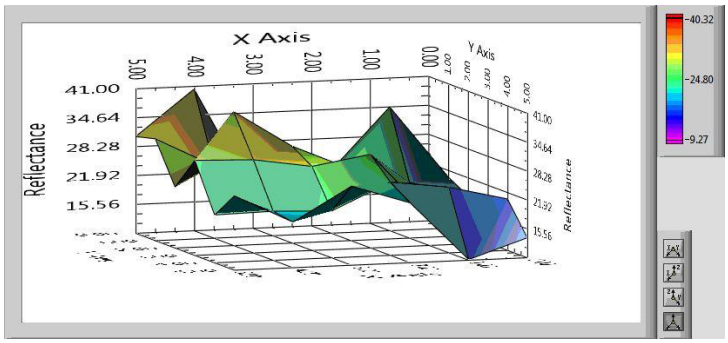

λ = 700 nm

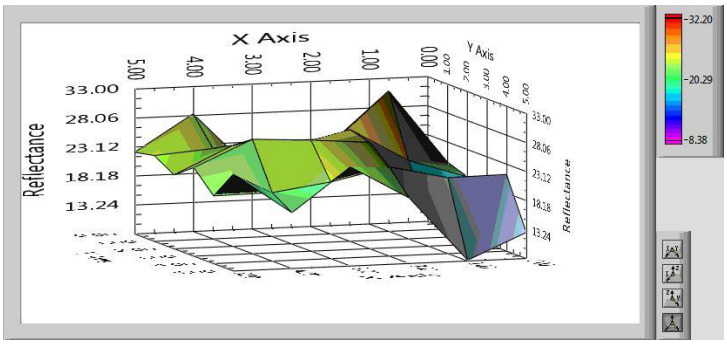

λ =650 nm

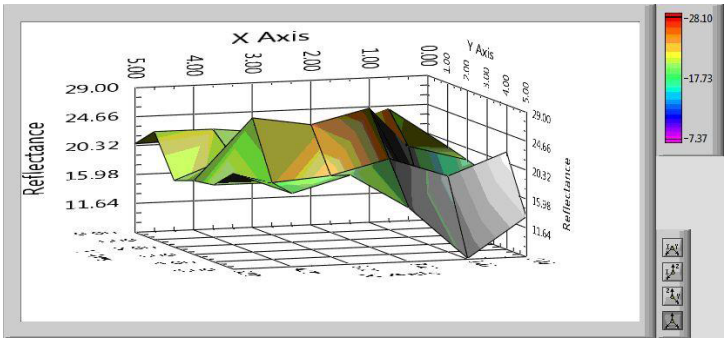

λ =600 nm

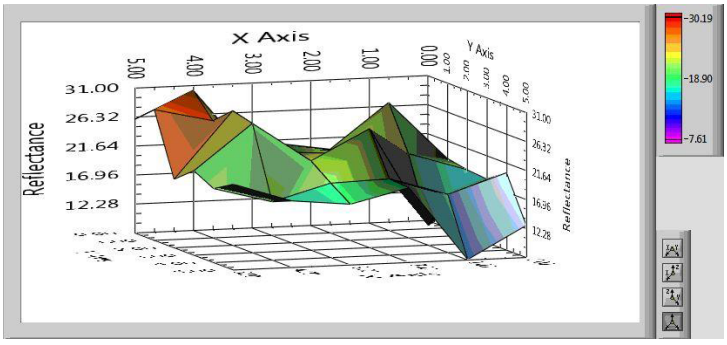

λ = 550 nm

Figure 7. Spatially resolved color/reflectance maps of a laser-treated stainless steel sample containing micron-scale color islands. A single island (of low average reflectance) is included in the bottom right corner of these maps.

A full spectral analysis was completed on islands versus surrounding areas (all treated with equal laser fluence). In general, the islands exhibited a low average reflectance with a minima in the range of 450 to 650 nm. An example of this is shown in Figure 8 with the lower (black) curve showing the results obtained from one representative island. A spectra obtained from a large area of this sample that includes islands and surrounding, non-islanded regions is shown in green (#1).

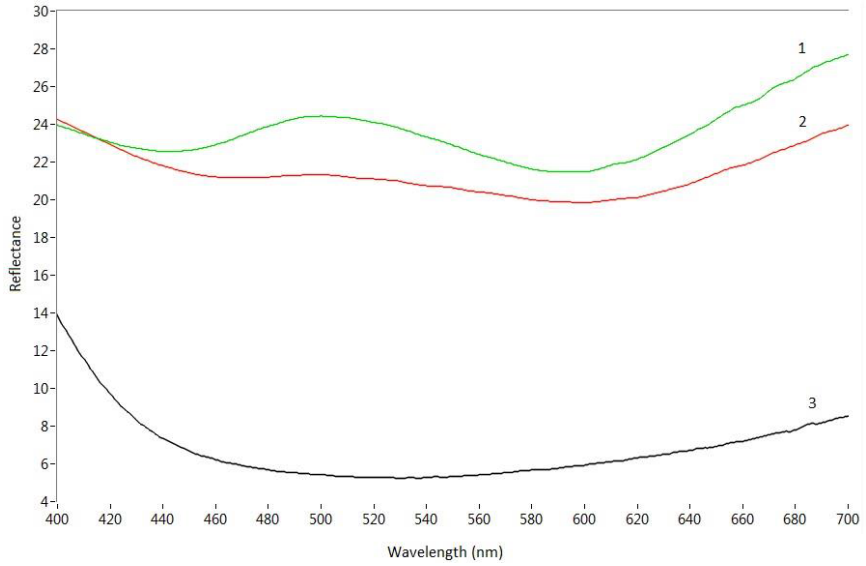

Figure 8. Spectral reflectance of two laser-treated stainless steel samples. The red curve is obtained from sampling a large area of a specimen not made containing color islands. The green and black curves are obtained from a sample containing micron-scale color islands. The black curve (#3) is obtained from a single island. The green curve (#1) is obtained from large area scans that include islands and surrounding non-islanded areas.

The green and red curves obtained from large-area scans show multiple interference maxima at different wavelengths compared with that formed on islands. Multiple maxima suggest a much thicker oxide in areas surrounding islands (or throughout the entire area of the oxide sample that does not form islands) compared with the oxide thickness associated with islands. Cross section scanning electron microscopy previously confirmed a reduced oxide thickness on microscale color islands (documented in last year's report). The different, measured chromaticities exhibited by islands on this sample are included in a plot (Figure 9). These are shown with red circles. The average chromaticity of the entire

colored feature is shown with a "+" symbol. Detectable differences are observed in additional to detectable difference in spectral reflectance.

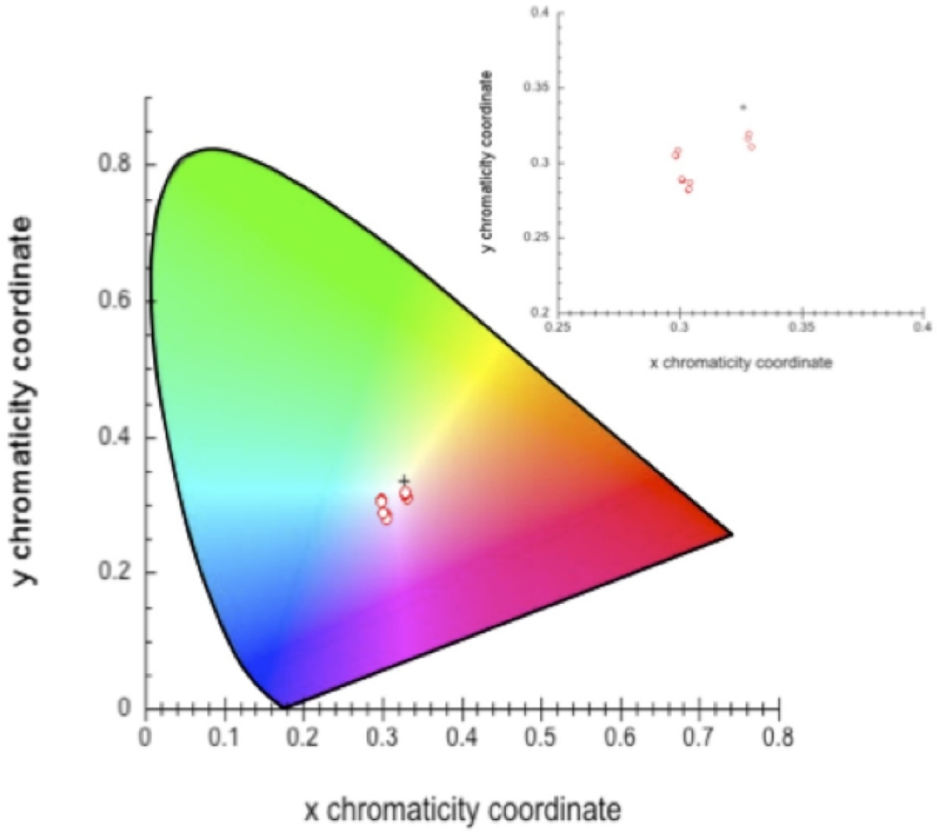

Figure 9. Chromaticities of discrete microscale color islands (shown with red circles) and the average chromaticity of the large area encompassing these, many other color islands and surrounding areas.

Key outcomes:

1.) Microspectrophotometry proved successful in resolving the distinguishing optical characteristics (i.e., spectral reflectance and color) of isolated, microscale islands compared to surrounding material.

2.) Differences in spectral reflectance and chromaticity were demonstrated for optically-identified color islands compared to the average properties of surrounding area.

3.) Laser color islands (with reduced average reflectance) generally have a decreased oxide thickness compared to surrounding areas. This is found for oxide layers made on stainless steel substrates.

4.) Spectroscopic ellipsometry was used to determine the optical constants of oxide layers produced on the surface of Cr and Ti. Results were correlated with characterized microstructure, morphology and composition to identify mechanisms giving rise to colored appearance. Color is explained in terms of the intereference of light scattered from the top and bottom surfaces of oxide layers combined with the absorbing effects of defects produced within the layers.

5.) Three new technical papers have been submitted for publication as a result of our research. These summarize the spectral response and optical properties of laser marked layers. These submissions are documented in the Metrics Chart.

Task 8: Investigate new laser fabrication techniques that produce color markings with improved corrosion resistance

Background:

In order to find use as intrinsic markings, laser-fabricated color markings must resist environmental degradation and wear.

Many of the laser color markings produced on steel substrates to date have proven susceptible to corrosion attack when immersed in a saline environment for long periods of time. In particular, laser colored steel samples immersed in concentrated salt water, as well as those set in salt fog atmospheres, have undergone severe corrosion after many days of continued exposure. Detailed microscopic studies confirmed that the thicker colored oxide layers grown on SS 304L using our traditional (single scan) laser approach were generally not protective in chloride-containing environments. This is because of the presence of through-thickness cracks in oxide layers, which allow contact with underlying Cr-depleted regions of the steel substrate. It is speculated that the residual stress and thermal shock associated with pulsed laser – stimulated growth leads to cracking.

There are a number of candidate approaches that could overcome this shortcoming and ensure the continued use of color markings made on steel substrates. For example, a transparent clear coat could be applied over markings in a way that prevents corrosion and keeps markings visible. Our team also envisions hybrid methods of laser processing that avoid cracking altogether. In particular, utilizing a multi-pass approach that builds up layers in steps could offset the large elevated temperatures associated with single pass processes, and reduce residual stress. Supplying additional Cr to the near surface volumes of substrates to offset corrosion is another potential solution that is beyond the scope of our research.

In previous years' research, we have investigated only single pass laser irradiation processes. The oxide thickness (intimately related to its color) was increased by lowering the scan speed of the moving beam. This would increase the accumulated laser fluence. In some cases, the oxide thickness made on stainless steel was hundreds of nanometers. Although residual stress could not be quantified, it can be expected that differences thermal expansion coefficients (substrate vs. film) could lead to a large, in plane biaxial stress.

Major activities:

In the past 10 months, we have investigated a different approach for fabricating color markings on stainless steel. The new approach utilizes multiple laser passes and a reduced pulse energy. The idea behind this is to build color oxide layers in steps rather than all at once. This should allow one to build oxide layers to the thickness required to obtain a given color. The potential benefits of multiple passes at reduced beam energy include the attainment of a given oxide thickness (and associated color) with reduced thermal excursions. It is thought that this may reduce the residual stress of the coating, which underlies cracking within.

Over the course of 10 months, we have fabricated oxide layers on stainless steel 304L using the aforementioned multi-pass method and tested these for corrosion resistance. Samples were compared directly with others made to similar oxide thickness using a traditional, single-pass process. All substrates were austenitic stainless steel 304L, with a composition in wt.% of 18.11% Cr, 8.00% Ni, 1.63% Mn, 0.42% Si, 0.14% Mo, 0.083 % N, 0.025% S and P, 0.023% C, with the balance as Fe. Polished samples were cleaned and then irradiated in air using an Er-doped, pulsed fiber laser from SPI Inc. Oxide layers with total thicknesses of 100, 200 and 300 nm were developed by multi-pass irradiation of the same area. Generally, the laser fluence was set to fabricate either 25 or 50 nm per pass (note: there was a reduced growth rate detected after the growth of a first layer). An average power of 5.6 W and a pulse frequency of 225 kHz was chosen to enable comparison to previous results. Hatch spacing was maintained at 10 μm throughout. Multiple samples were made using a given recipe to enable parallel environmental testing paths.

Additional austenitic stainless steel 304L coupons were made using our traditional single pass approach, for side-by-side testing and comparison. Oxide layers were made to the same final thicknesses produced using a multi-pass approach (i.e., 25, 75, 100, 125, 200, and 300 nm).

Testing involved salt spray testing and anodic polarization. Samples were prepared for salt spray testing by applying an enamel boundary around color markings to ensure that only laser-irradiated areas were exposed to the corrosive environment. Salt spray testing was performed in accordance with the ASTM B117 standard for 168 hours. Polished blank (unmarked) pieces of SS304L were used as controls. Anodic polarization tests were conducted on samples to evaluate the pitting corrosion resistance and general localized corrosion behavior of the different substrate-oxide samples. Anodic polarization tests were performed with a conventional three-electrode cell, with a Pt counter electrode and a Ag/AgCl reference electrode, using a Gamry DC105 corrosion test system. Polarization curves were produced in a 3.5% NaCl solution at a sweep rate of 0.5 mV/s after stabilization of the open circuit potential.

Immersion testing (within solution) was not attempted. After exposure, samples were rinsed and dried prior to microscopy.

Specific Objective(s):

The specific objective for the previous year was the following:

- Investigate new laser fabrication techniques that produce color markings with improved corrosion resistance (Task 8)

Significant Results and Findings:

Salt Spray Testing

Salt spray testing showed that multilayered oxide samples are still susceptible to corrosive attack but exhibit improved corrosion resistance. A corrosion product deposits on the surface of all oxides, as shown in Figure 10a-d. The most pervasive corrosion product developed on the surface of the 5-layer and 12-layer oxides. The deposition of a corrosion product indicates that the oxides are not impervious to chloride containing solutions. Likely, the substrate melt zone is likely still depleted of Cr after laser processing, even for the thinnest films.

Two sets of images are used to qualitatively contrast the corrosion occurring after 168 hours of salt spray exposure. In Figure 10, we include optical micrographs of four different oxide layers. Each of these colored features were made using our traditional single pass laser approach. Severe corrosion has occurred in each experiment. In Figure 11 we include optical micrographs obtained after the exposure of oxide layers created by multiple passes. The left column of this figure shows micrographs obtained after corrosion testing, whereas the right column shows the same areas after cleaning the same areas with oxalic acid. Qualitatively, it is found that less corrosion product is produced from multi-layered films – a first indication that these are more resistant to environmental degradation. Inspection after removal of the corrosion product (Fig. 11 d-f) demonstrates that the laser-fabricated oxides are still intact although the surface reflectance is changed.

In general, the thinner oxide layers proved more corrosion resistant. Figure 12 includes two electron micrographs after corrosion testing of two samples. Figure 12 (a) demonstrates no surface degradation for an oxide layer made using 3 laser scans after salt fog exposure. Figure 12 (b) shows severe oxide dissolution in an oxide layer sample made with 12 laser scans. The differences are likely

due to the fact that no cracks form in the thinner oxide layer. The residual strain energy in this oxide is not sufficient to crack the oxide layer. Thus, there is no open path for corrosion attack of underlying Cr-denuded zones.

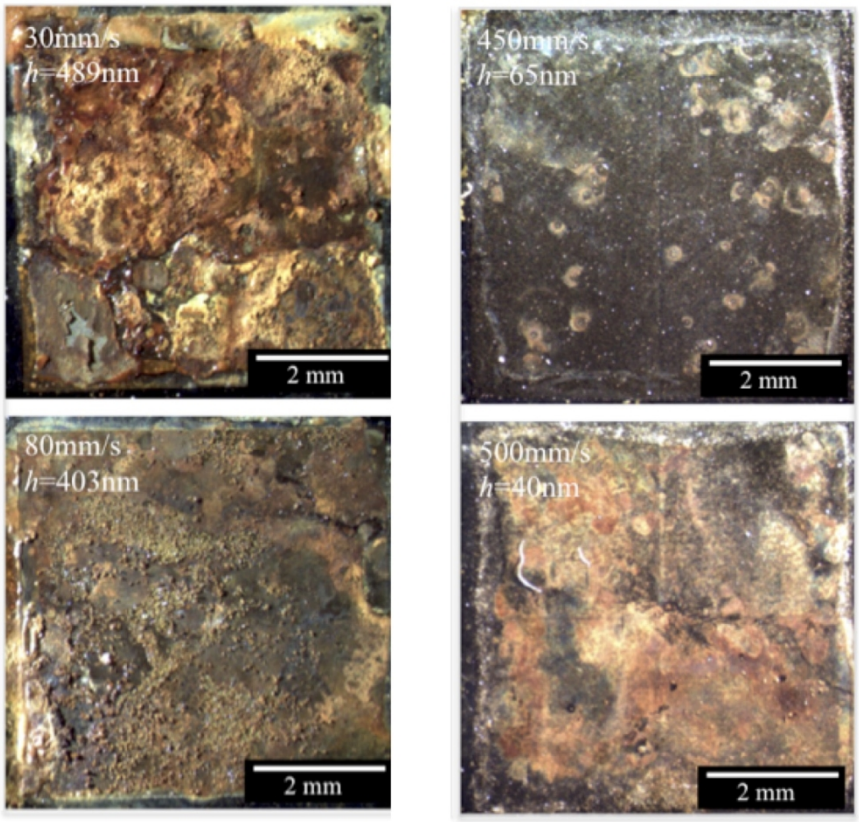

Figure 10. Optical micrographs of four oxide layers subjected to 168 hours of salt spray exposure indicating severe corrosion. Each of these oxide features was made using our traditional single-scan laser approach. Oxide layer thicknesses (h) are specified above along with the scan speed for laser processing.

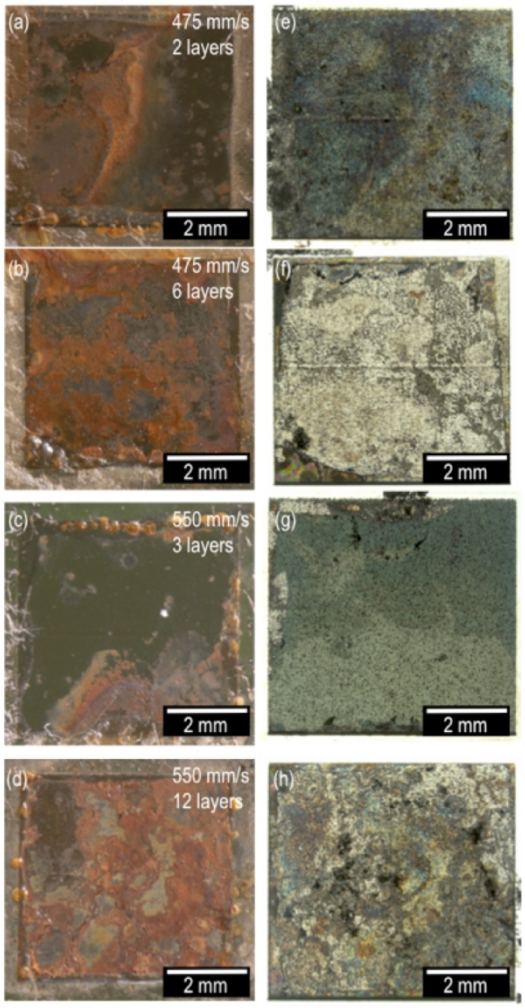

Figure 11. Optical micrographs of multilayered oxides after 168 hours of salt fog exposure (a-d) and the same features following oxalic acid cleaning. The number of scan passes used to create a given feature is specified in the left images. The laser scan speed is also specified.

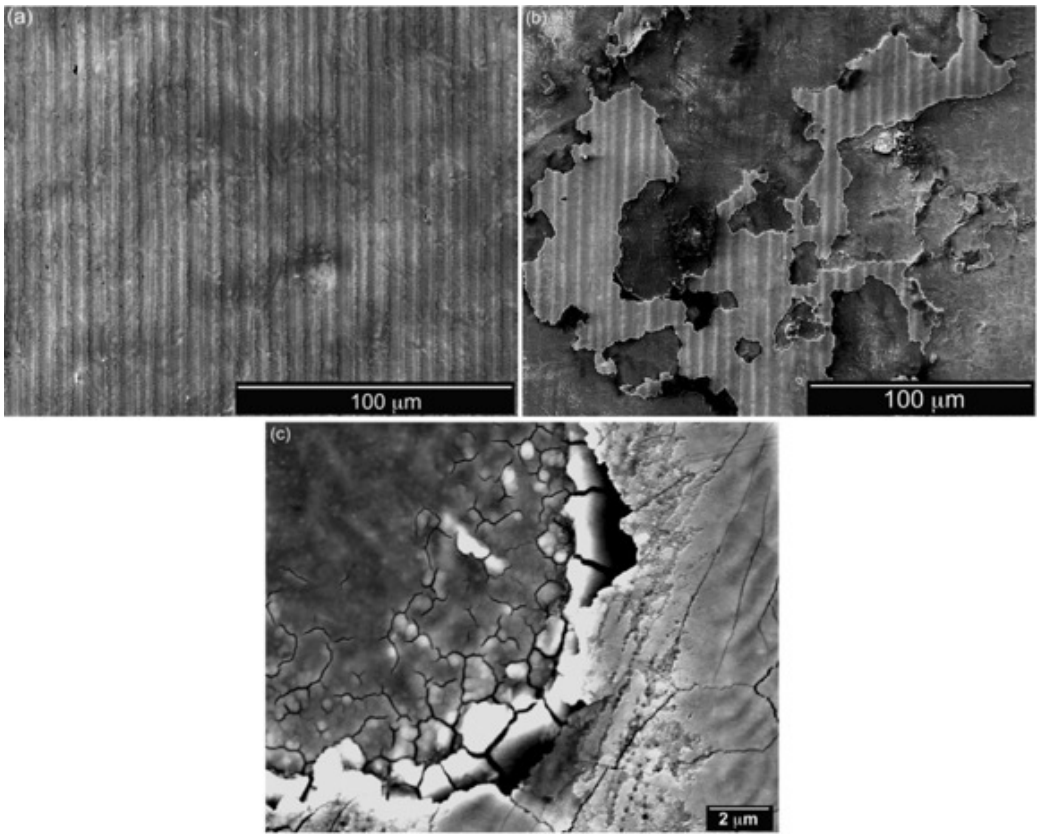

Figure 12. Electron micrographs of a 3-layer oxide (a) and a 12-layer oxide (b) after salt fog exposure and subsequent oxalic acid cleaning. No surface degradation is apparent for the 3-layer film, conversely, the 12-layer coating shows severe oxide dissolution; surface channel cracks are still apparent, as shown in (c).

Potentiodynamic Testing

Additional anodic polarization tests showed that multi-layered oxide coatings are susceptible to corrosion, but are still improved when compared to oxides made using a single laser pass process. In Figure 13 below, we include optical micrographs of samples subjected to anodic polarization tests. These particular layers were made with our traditional single-pass approach and act as a baseline for comparison to oxides made with new processes. Images a-e show initial sample surfaces prior to testing, and images d-j show degradation of the same samples after testing, in which pitting has occurred. The oxide thickness (h) is specified in the figures along with the laser scan speed used to fabricate a given feature. The images on the right show degradation of the surface. Anodic polarization causes pitting and dissolution of the oxide film and localized corrosion of the substrate. Stainless steel is known to be susceptible to pitting at low potentials in chloride containing solutions; thus there is some pitting even when using raw material. More extensive pitting is exhibited in these laser-treated (oxidized) samples.

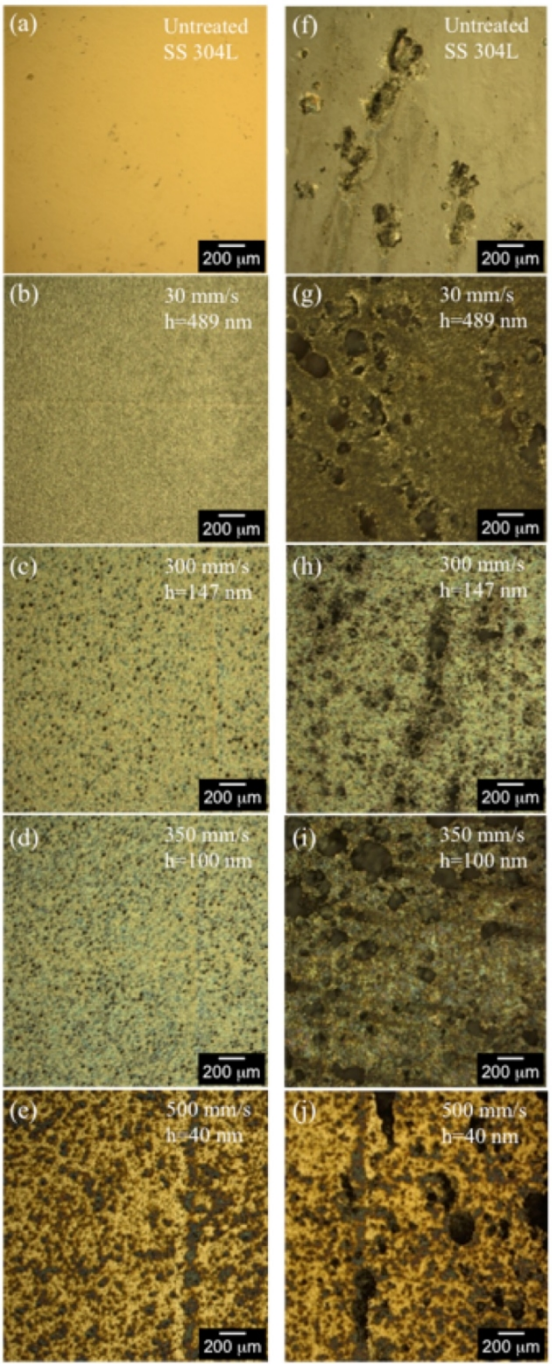

Figure 13. Optical micrographs showing samples subjected to anodic polarization tests. Images a-e show samples prior to testing. Images d-j show degradation after testing. The top two images are a control SS304L samples that was not laser color marked. Within the images (b-e, g-j), an oxide layer thickness is specified along with the associated laser scan speed where appropriate. All color layers shown here were made by a single laser pass process.

With Figure 14, we include the measured corrosion potential of two oxide samples along with the base metal (not treated by laser irradiation). These tests demonstrate that corrosion potential varies directly with oxide thickness; thicker oxides are the most susceptible to pitting corrosion. In light of post-mortem microscopy, the propensity to crack tracks with the prevalence of channel cracks. With the plot

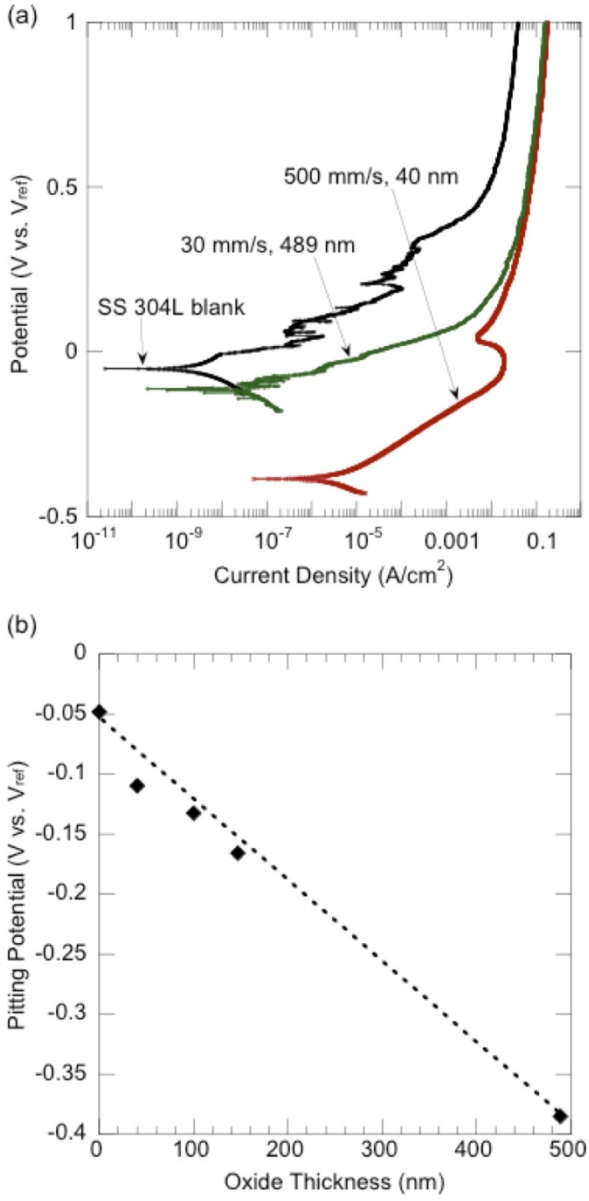

Figure 14. (a) Anodic polarization curves obtained from testing a SS304L control sample (not treated by laser irradiation) as well as two samples having laser grown oxide layers. Oxide layer thicknesses (489, 40 nm) and scan speeds are specified for the two laser color marked oxide layers. (b) Plot of corrosion potential as a function of measured oxide layer thickness.

in Figure 14 (a), one sees that the 489 nm – thick oxide layer shows no passivation behavior, but instead begins to dissolve immediately after the corrosion potential is reached. The corrosion potential for this oxide shifts to a more cathodic value than that exhibited by the thinner oxides, consistent with a higher corrosion rate. It is likely that this particular sample has a larger Cr-denuded zone and channel cracks in the oxide all the electrolyte to penetrate exposing the Cr-depleted portions of the substrate.

Finally, it is found that oxide layers made with multiple, low energy laser passes are generally superior to those made with single passes. Examples of potentiodynamic-tested oxide films made by multi-pass laser scanning are shown in Figure 15. Images capture the films before and after testing; for brevity, only oxide layers grown using scan speeds of 475 mm/s and 550 m/s are included. In general, these oxides show no improvement in localized corrosion resistance compared with the untreated steel, as the corrosion potentials for all laser-treated samples are more cathodic than for SS304L (bare). However,

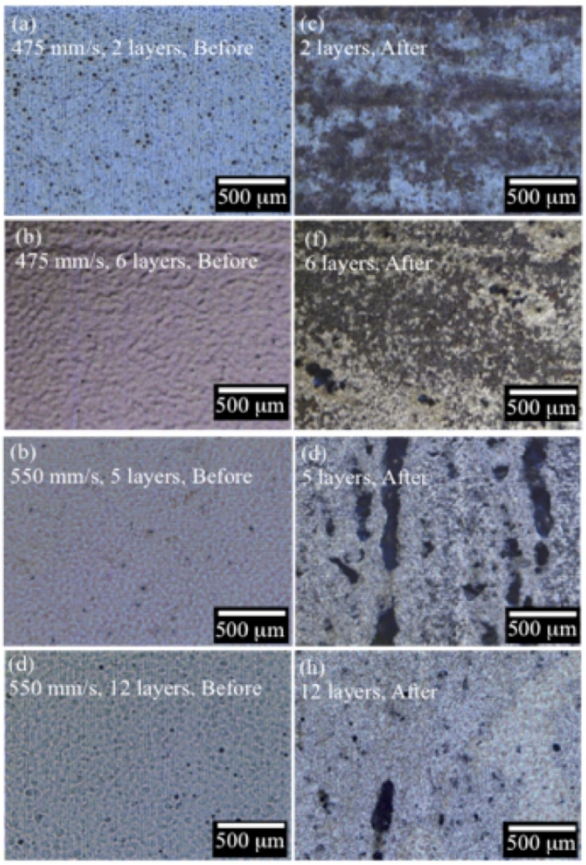

Figure 15. Optical micrographs subjected to anodic polarization tests. Images a-d show samples prior to tests. Images e-h show degradation after testing. Within images, the number of laser scans used to grow the feature and the scan speed are specified. Color oxides shown were made using multi-scan processes.

these particular laser-treated samples are less susceptible to localized corrosion attack compared with oxide layers made using a single-pas approach. Evidence for this is found in comparing the micrographs of Figs. 13 and 15. There are less number of pits per unit area in the oxide layers made with multiple passes.

Additionally, a more quantitative difference in susceptibility to localized corrosion comes from measured corrosion potentials. Compared to the corrosion potentials shown in Figure 14 for single – pass fabricated oxide layers, the oxide layers constructed using multiple laser scan passes exhibit a much smaller cathodic shift in potential. For example, the 100 nm oxide films made using multiple laser scan passes were measured to have a corrosion potential of -0.07 V vs. V_{ref}.

Key outcomes:

- Nanosecond pulsed laser irradiation can be successfully employed to fabricate layered oxide coatings which are both mechanically robust and resist environmental degradation.
- Colored oxide coatings fabricated on SS 304L using modified, multi-pass laser heating processes to investigate their corrosion resistance. Individual layer thicknesses formed during a single pass were kept small, but final layer thickness encompassed the range of thicknesses generated previously for colored films. Layered films grown using a reduced laser scan rate tended to be more resistant to both localized and general corrosion than oxides fabricated with a scan rates in excess of 500 mm/s.
- Though the laser colored, steel substrates are still susceptible to corrosion in a chloride-containing environment, any corrosion product that deposits on the surface of the color oxide pattern can be removed by cleaning with oxalic acid. Importantly, the laser-fabricated oxide is still present on the surface after salt spray exposure and cleaning.
- Three presentations were delivered at International Conferences in the fall of 2014 summarizing our work on this task. These are documented in the Metrics file within the Presentations table.

Task 9: Research new methods for laser marking curved surfaces

Background:

All of our previous laser color marking activities and research (prior to 2015) involved a laser scan head that was capable of patterning colored features over small, planar areas. Typically, a focused beam was swept across a sample with the total patterned areas limited to ~ 16 cm^2. Scanning outside this region was possible however the beam was defocused making it insufficiently intense to cause oxidation.

Major activities:

Knowing that critical assets may require larger intrinsic markings and recognizing that a majority of components are non-planar, our team has investigated new compact scan head technology that enables laser color marking over large areas including those on nonplanar surfaces.

We have learned that Nutfield, Inc. has expanded their current product set to offer a different scan head that allows one to laser color mark much larger areas up to 1 m^2. The instrument (referred to as the 3XB series) is a compact scanning solution that offers 3-axis capability at a cost comparable to 2-axis systems. This means the scan head provides a new capability to laser mark curved surfaces, such as a cylinder, sloped solid, etc. A photograph of this device is included in Fig. 16 below.

Figure 16. Nutfield Technology's 3-Axis Contour designed for laser color marking large surface area and shaped (nonplanar solids). Enclosure is roughly 30 x 30 x 70 cm. https://www.nutfieldtech.com/3xb-3-axis-scan-head/

Specific Objectives:

The specific objective for the previous year was the following:

- Research new methods for laser marking curved surfaces (Task 9)

Significant Results and Findings:

Although arrival in our laboratory was delay, this instrument is now (as of last month) installed and tested in our laboratory for laser color marking. Initial demonstrations have included basic laser color marking of planar stainless steel substrates over 400 cm^2 areas. Experiments that laser color mark large-diameter, cylindrical Ti6Al4V rod without rotating the work piece are also underway. In this case, it is anticipated that areas on the substrate with direct line of sight to the steering mirror can be irradiated with laser light.

Key outcomes:

The key outcomes of this task are as follows:

- A new instrument inspired by our research team (called the 3XB series compact scan head from Nutfield Technologies) was successfully installed in our laboratory. Tests are underway with this new capability.
- Initial tests have demonstrated an ability to laser color mark large stainless steel 304L across surface areas up to 400 cm^2.
- The new compact scan head has proven compatible with the nanosecond pulsed, 1064 nm laser currently being used by our team for laser color marking.

Task 10: Complete model simulations of laser-induced ripple formation

Background:

Periodic surface ripples formed by scanned, pulsed laser irradiation are of interest as a second form of intrinsic marking. We identify that these markings , much like colored, microscale islands, can be randomly located (or have elements of randomness within) even when a beam is scanned uniformly across a surface. Once cataloged, these types of features could prove useful for assuring the authenticity of critical assets and protecting against counterfeiting and substitution.

Formed by scanning an ultrashort-pulsed laser beam across a component's surface, periodic ripples generally develop as the beam encounters local maxima on a surface. The characteristic periodic features can be cataloged in terms of their location (if forming sparsely across a surface), their amplitude or their average ripple wavelength. Previously, our work on laser-induced periodic features demonstrated that surface asperities (roughness) must be present to create periodic surface ripple patterns upon laser irradiation. A rough hill-and-valley surface, such as that produced from mechanical machining, provides many sites for light scattering and interference, which underlies the formation of periodic morphologies near asperities.

Documented in last year's report, our team experimentally investigated the creation of periodic ripple patterns resulting from laser irradiation of a well-defined step edge. This set of control experiments was designed to remove confounding artifacts such as cratering and variable surface roughness and thereby focus on and identify the fundamental light-solid interactions that govern ripple formation and their intriguing characteristics. A key observation from last year's experiments is that the period (i.e., wavelength) of laser-induced surface ripples varied with both the fluence and the polarization direction of the incident light. Based on these observations, we hypothesized that periodic surface structures are formed from the combined effects of Fresnel diffraction and surface plasmon polariton excitation.

Major activities:

In order to confirm our hypothesis and develop an improved understanding of why surface ripples form, we have completed predictive model simulations using an Electromagnetic Solver (COMSOL). This numerical modeling approach has investigated the relative roles of beam characteristics such as (peak intensity, light polarization, wavelength) and expanded this to study the potential role of surface plasmon polaritons, Fresnel diffraction and other potential effects.

Generally, we reproduce in the model the key characteristics of the incident single pulse of laser light. Also, the single step edge structure (constructed in the laboratory by photolithography, sputter deposition and liftoff) is included. This has more often involved a ~100 nm high Au mesa structure on Si although our recent models have expanded to include additional materials. Once constructed, the EM solver predicts how the electric field varies across all surfaces. Figure 17 depicts some of the key characteristics of the model.

It is surmised that the periodic, intensity maxima present on the surfaces correlate with the selective ablation/evaporation of material from different sites on a surface that results in a periodic ripple morphology. Thus, conditions, such as intensity and polarization were intentionally varied to match experiments and compare.

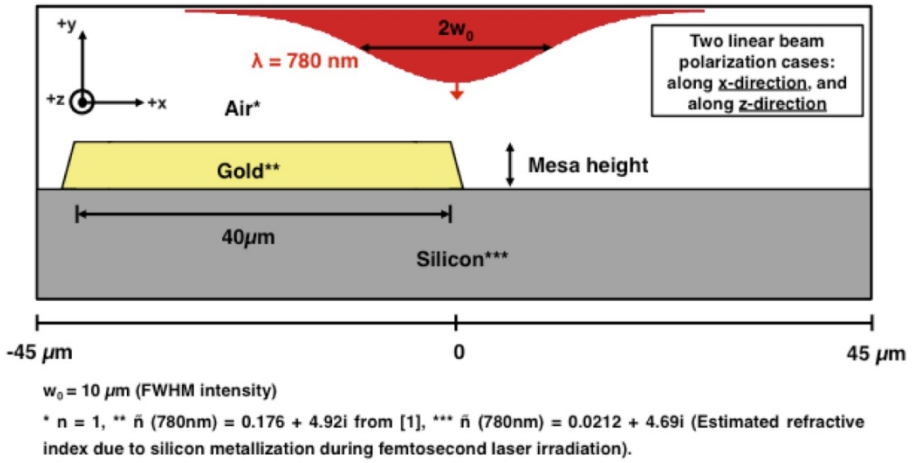

Figure 17. Characteristics of the incident laser beam and starting surface structure included within our predictive model simulations and general nomenclature therein. These generally match the characteristics used prior experiments.

To recall from last year's report, Figure 18 shows an example of periodic surface ripples formed near the edge of a Au mesa structure (on Si) after irradiation by a single pulse of ultrashort (150 femtosecond) 780 nm light. In this example the laser spot was centered over the mesa edge. A periodic ripple patterned is evident in this tilted view with ripple wavevector oriented horizontally. As with all laser process conditions used here, the amplitude of the ripple pattern decays with distance away from the step edge.

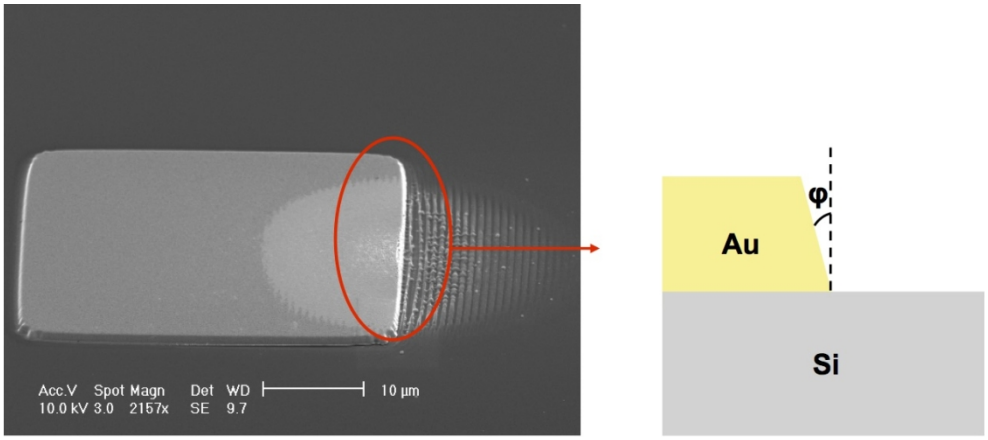

Figure 18. The scanning electron microscope image on the left shows a Au mesa structure after single pulsed laser irradiation. The depiction on the right reports that our mesa structures have a measurable sidewall angle which is found to be important to the produced ripple characteristics.

Specific Objectives:

The specific objective for the previous year was the following:

- Complete model simulations of laser-induced ripple formation – involves an ElectroMagnetic field solver (Task 10)

Significant Results and Findings:

Taking into account the various structural/compositional details of initial surfaces and the shape, size, pulse duration, etc. of incident light, our model simulations have successfully predicted periodic variations in electric field intensity that share many of the same characteristics of produced ripple patterns.

Generally, the electric field variations are produced because of Fresnel diffraction. A portion of the incoming pulsed light is diffracted from the edge of the mesa. Interference of waves is seen in Figure 19 both at the surfaces of the specimen and in free space. Results are shown in Figure 19 for different mesa heights, which strongly affects the intensity at the surface. Also evident in these figures nonzero sidewall angles have an effect on the intense variations in electric field present at surfaces. In particular, a tapered sidewall leads to a much stronger average intensity variation for the case of the 585 and 780 nm tall mesas. Note: the sidewall is taken to be representative of that measured in experiments by scanning electron microscopy.

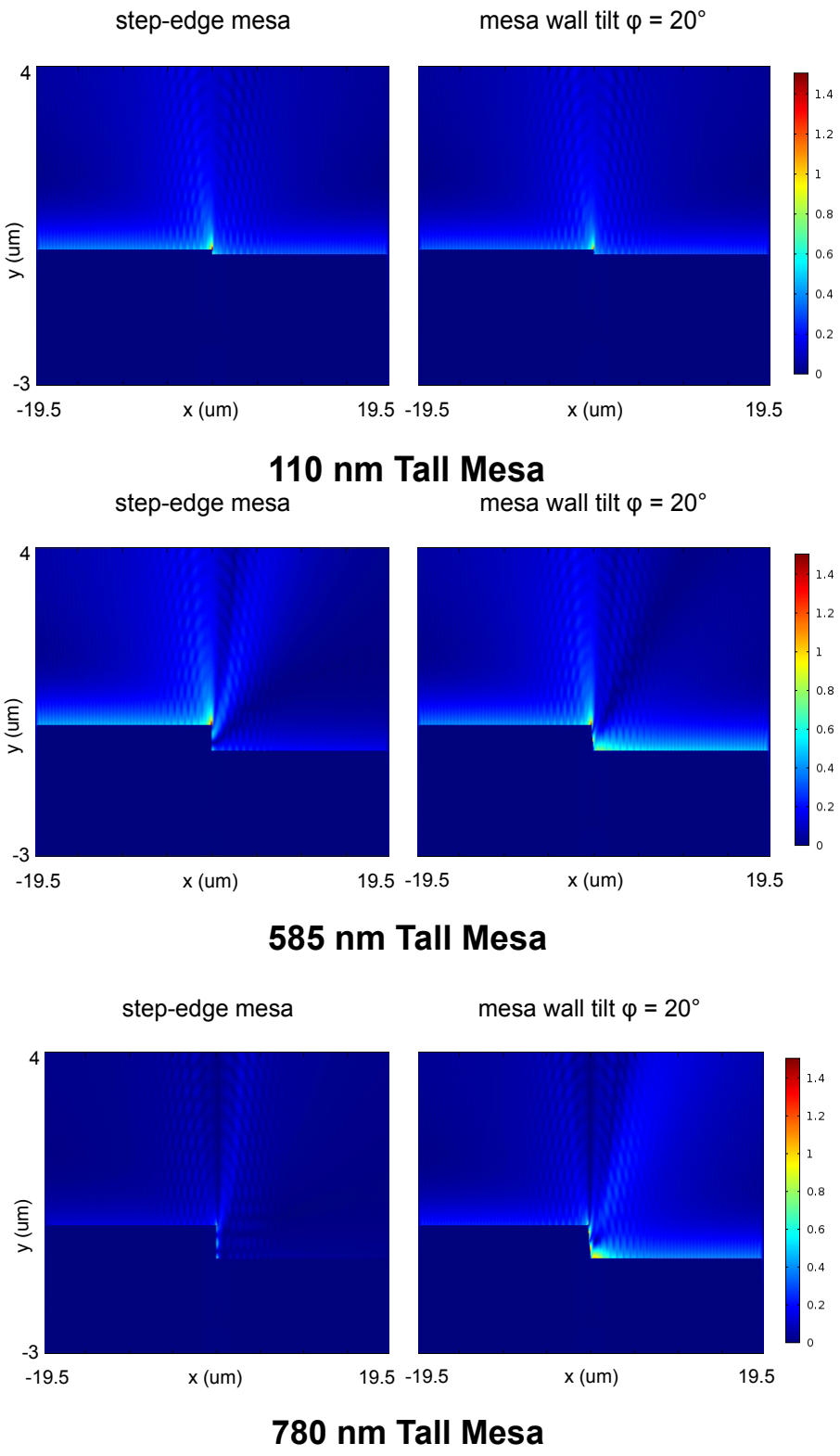

Figure 19. Model predictions of electric field variations (shown in cross section) across a mesa structure of a given, specified height. Two cases are shown for each mesa including vertical sidewall steps (shown

on left) and those having a 20-degree sidewall angle. In each representation, the mesa is shown on the left and the lower surface (Si) is shown on the right.

Several characteristics of periodic ripple structures predicted by model simulations were validated in the laboratory through measurement. For example, model simulations has been used to predict the variations in electric field intensity across a Si and Au surface for different polarization directions. In Figure 20, results are shown for the case wherein the polarization direction is oriented perpendicular with respect to the irradiated edge of a mesa. Furthermore, the average period of the electric field (on both surfaces) is less than the wavelength of incident light. The two bottom plots (one for Au surface and one for Si) show a decreasing amplitude with distance away from the edge, consistent with the general effect shown in Figure 18. Variations are, additionally, predicted in Figure 20 as a function of mesa height. Of note, there are mesa heights (390 nm and 720 nm) wherein predicted amplitudes (on Au) are minimal.

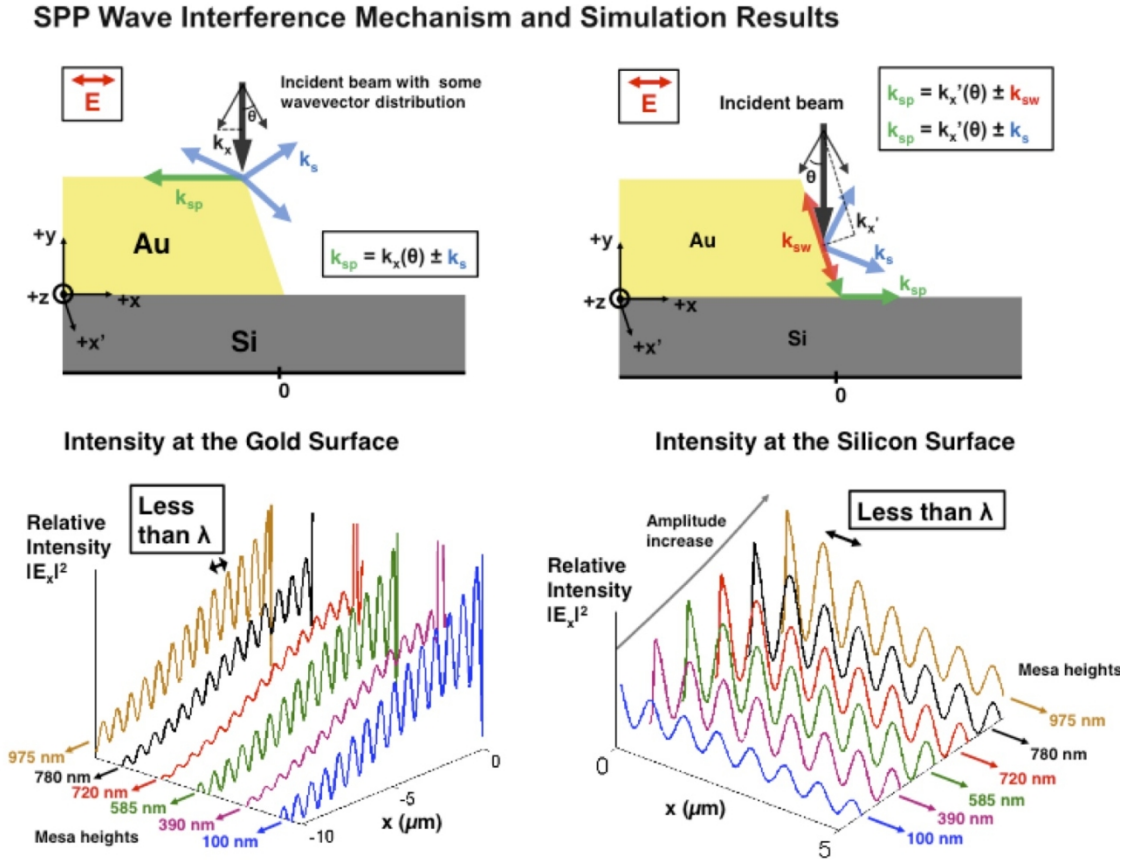

Figure 20. Model predictions of electric field variations as a function of mesa height for the case where incident, pulsed light is polarized with a wavevector that is aligned perpendicular to the mesa edge (oriented into the page of this drawing). Results shown include the intensity variations on the Au and on the lower Si surface.

Laboratory experiments have been used to validate many of the model predictions. For example, two sets of results are shown in Figure 21 that are quite consistent with the aforementioned model results for the case considering polarized light oriented perpendicular to a step edge. On the left is the experiment involving a 100 nm high Au mesa. Ripples are formed on both Si and Au, with those on Si being more prevalent (similar to model predictions). Other consistent features include a decaying amplitude away from the step edge on both Au and Si. Of note, the measured period of this rippled morphology is less than the incident wavelength of pulsed light (780 nm, shown in red in the graph).

The experiment shown on the right side of Figure 21 similarities and differences that are each consistent with model predictions. Again amplitude decays away from the edge as in the 100 nm case and the average period is suppressed compared with the incident wavelength. In addition, no evidence of ripples is found on the Au for the case of the 720 nm high structure. Recall from Figure 20 that this is a height, that is predicted to produce minimally varying electric field intensity on gold.

In general, one of the most recognizable features of ripples (and one that is likely to vary when a focused laser beam is scanned across a rough surface) is its period. In the case of the models and experiments in Figures 20 and 21, the conditions are optimized for surface plasmon polariton generation. The alignment of the polarization gives rise to collective electron excitation which can distort the local electric field. For this reason, we argue that both models and experiments support our hypothesis that surface plasmons affect diffracted laser light in such a way as to decrease the period of electric field variations, and this leads to a reduced ripple wavelength.

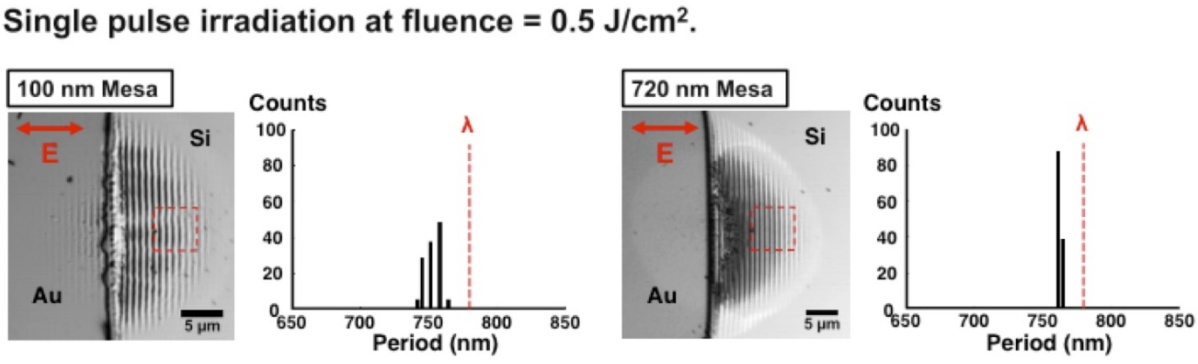

Figure 21. Results from validation experiments involving two different mesa heights, 100 and 720 nm. Plan view images show the formed ripple patterns produced on Au and on Si after single pulse irradiation. In these two experiments, the polarization direction is aligned normal to the irradiated mesa edge as shown. Plots next to each image summarize measured ripple periods. This example shows ripple periods that are less than the wavelength of incident light, which is consistent with model predictions.

Additional model simulations and validation experiments have been completed to explore the opposite polarization orientation, one in which its direction is aligned parallel to a linear mesa edge. Results from model simulations are shown in Figure 22.

Model simulations again show that electric field intensity should vary across the surface – an effect of Fresnel diffraction. In addition, similar to the earlier case, ripple amplitude decays with distance away from a step edge. Nevertheless, there are several differences noted. On the right, the plot shows that the period of electric field variations is of the order of the incident light wavelength with some variation along the path. This is different than the previous case, which was optimal for surface plasmon generation.

Validation experiments shown in Figure 23 demonstrate many of the predicted characteristics. The ripple period was measured by Atomic Force Microscopy (AFM) and found to be equal (on average) to the wavelength of incident light, although some variation was found. With this similarity and knowing that conditions are not optimal for collective electronic excitations, Fresnel diffraction is thought to be largely responsible for formed patterns.

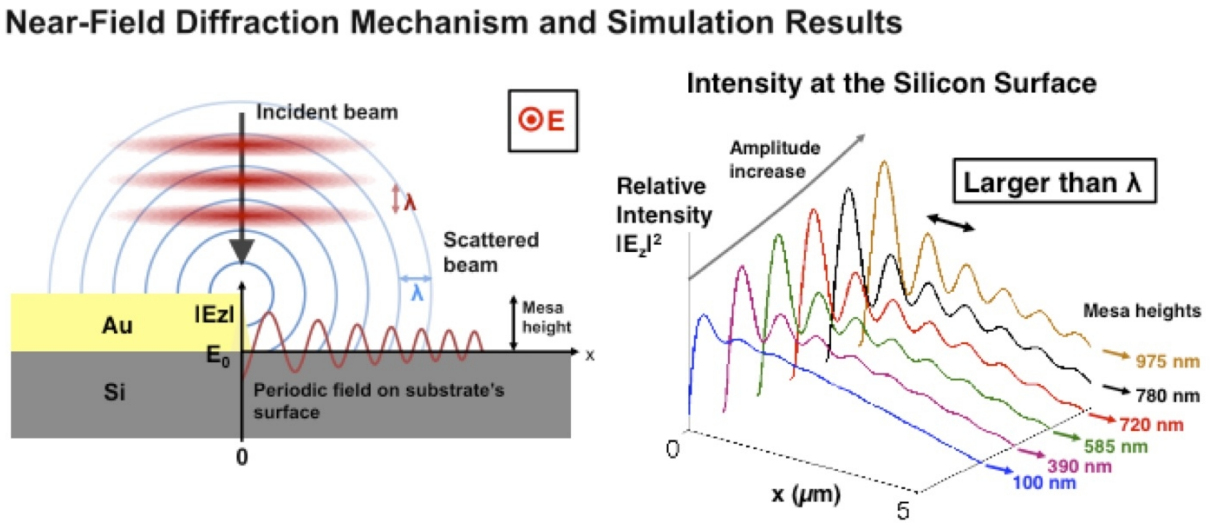

Figure 22. Model predictions of electric field variations as a function of mesa height for the case where incident, pulsed light is polarized with a wavevector that is aligned parallel to the mesa edge (oriented into the page of this drawing). Results shown include the intensity variations on lower Si surface.

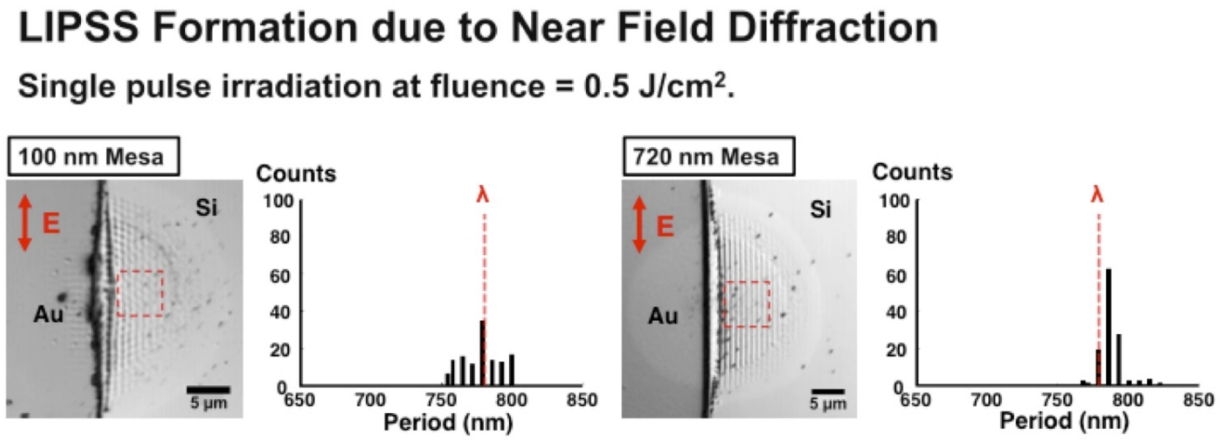

Figure 23. Results from validation experiments involving two different mesa heights, 100 and 720 nm. Plan view images show the ripple patterns produced on Au and on Si after single pulse irradiation. In these two experiments, the polarization direction is aligned parallel to the irradiated mesa edge as shown. Plots next to each image summarize measured ripple periods. This example shows ripples whose mean period is equal to the wavelength of incident light - consistent with model predictions.

Key outcomes:

- Model simulations and experiments demonstrate that periodic surface ripples form when short or ultrashort pulsed laser light strikes a rough surface. Further, the characteristics of the produced ripple pattern vary significantly according to the height and alignment of the hill-and-valley surface morphology initially present. Thus it can be expected that a scanned laser beam will act with a rough surface in various ways to produce largely-randomized ripple patterns.
- Model simulations reveal that the origin of periodic surface ripples is Fresnel diffraction (interference) and that surface plasmon polaritons can affect the characteristic shape of the produced surface morphology.
- Model simulations predict periodic electric field variations are produced when ultrashort pulsed laser light is incident on a step edge, consistent with experiments.
- Model simulations predict that the amplitude of the periodic electric field variations is decreased with distance away from the mesa edge, consistent with experiments.
- Model simulations predict that the period of the electric field wave on a surface is less than the wavelength of incident light when conditions are ideal for surface plasmon polaritons. This is consistent with experimental observations of decreased ripple period when the polarization direction of incident light is oriented perpendicular to the mesa step edge.

- Model simulations predict that the period of the electric field wave on a surface is approximately the same as the wavelength of incident light when the polarization direction of incident light is oriented parallel to the mesa step edge.
- A poster presentation was delivered at the SPIE Photonics West Conference on Laser based micro- and nano-processing in San Francisco. Information is provided in the Metrics chart.

What opportunities for training and professional development has the project provided?
If the research is not intended to provide training and professional development opportunities or there is nothing significant to report during this reporting period, state "Nothing to Report." Describe opportunities for training and professional development provided to anyone who worked on the project or anyone who was involved in the activities supported by the project. "Training" activities are those in which individuals with advanced professional skills and experience assist others in attaining greater proficiency. Training activities may include, for example, courses or one-on-one work with a mentor. "Professional development" activities result in increased knowledge or skill in one's area of expertise and may include workshops, conferences, seminars, study groups, and individual study. Include participation in conferences, workshops, and seminars not listed under major activities.

Regarding professional development, our graduate students Samantha Lawrence (Purdue) and Rico Cahyadi (Michigan) were able to attend technical conferences, describe their work and interact with others knowledgeable in their field of study. Samantha Lawrence attended the Gordon Conference on Mechanical Properties of Thin Films and presented her work as a poster entitled "Development of Mechanically and Environmentally Stable Oxide Coatings using Pulsed Laser Irradiation". While in attendance, she participated as discussion leader of the Gordon Research Seminar. This participation can be viewed at: http://www.grc.org/programs.aspx?year=2014&program=grs_thnflm. In December, 2014 she graduated from Purdue University with a PhD in Materials Science & Engineering. Rico Cahyadi delivered his first presentation at the SPIE Photonics West Conference on laser-based micro-and nano-processing (San Francisco). DTRA support was acknowledged in each case.

How have the results been disseminated to communities of interest?
If there is nothing significant to report during this reporting period, state "Nothing to Report." Describe how the results have been disseminated to communities of interest. Include any outreach activities that have been undertaken to reach members of communities who are not usually aware of these research activities, for the purpose of enhancing public understanding and increasing interest in learning and careers in science, technology, and the humanities.

Our work was disseminated at several professional society symposia.

Our University of Michigan graduate student (Rico Cahyadi, Applied Physics) presented a poster at the SPIE Photonics West (Conference on laser-based micro-and nano-processing, San Francisco). The title of his presentation is "Structural Dependence and Mechanisms of LIPSS Formation at a Step Edge due to Single-pulsed Femtosecond Laser Irradiation". This research is a specific accomplishment for Task 10, mentioned above.

Samantha Lawrence delivered a platform presentation at the fall conference Materials Science and Technology 2014 in Pittsburgh, PA, entitled "Development of Mechanically and Environmentally Stable Oxide Coatings using Pulsed Laser Irradiation". She also presented a poster at the Gordon Research Conference on Thin Film and Small Scale Mechanical Behavior in Waltham, MA (same subject was discussed). This research is a specific accomplishment for Task 8, mentioned above.

Neville Moody delivered an invited presentation at the 2014 Materials Science & Technology Conference (Pittsburgh) entitled "Assessing the Role of Adhesion and Fracture on the Performance of Thin Film Systems".

With regards to published reports, we have submitted three new manuscripts for publication in peer-reviewed journals. These are currently being reviewed for publication.

This includes the following articles:

1. The Sensitivity of Laser grown Ti-oxide System Optical Properties to Layer Composition and Structure, Thin Solid Films, R.D. Murphy, D.J. Saiz, M.A. Rodriguez, P.G. Kotula, D.P. Adams, 2015.

2. Laser Grown Ti-oxide Films Exhibiting Memristive Behavior, Journal of Appl. Phys., R.D. Murphy, R.S. Goeke, D.J. Saiz, D.P. Adams, 2015.

3. The Optical and Structural Properties of Cr-oxide Films fabricated by Pulsed Laser Oxidation, Surf. and Coat. Technol., R.D. Murphy, D.J. Saiz, M.A. Rodriguez, P.G. Kotula, D.P. Adams, 2015.

Sandia's Technical Business Development Specialists have, over the course of the past 10 months, disseminated our accomplishments to various U.S. companies that may make use of this technology. Several have expressed interest in the Intellectual Property derived from this DTRA-funded research. Continued dissemination is expected.

What do you plan to do during the next reporting period to accomplish the goals?
If there are no changes to the agency-approved application or plan for this effort, state "No Change." Describe briefly what you plan to do during the next reporting period to accomplish the goals and objectives.

The project will end in September 2015. Thank you again for the opportunity to complete this research.